# Modification of Porous Alumina Membranes Using $Al_2O_3$ Atomic Layer Controlled Deposition

A. W. Ott, J. W. Klaus, J. M. Johnson, and S. M. George*

*Department of Chemistry and Biochemistry, University of Colorado, Boulder, Colorado 80309*

K. C. McCarley and J. D. Way*

*Department of Chemical Engineering and Petroleum Refining, Colorado School of Mines, Golden, Colorado 80401*

*Received July 17, 1996. Revised Manuscript Received November 25, 1996*[⊗]

$Al_2O_3$ films were deposited with atomic layer control inside the pores of Anodisc alumina membranes. To achieve this controlled deposition on a high aspect ratio structure, a binary reaction for $Al_2O_3$ chemical vapor deposition ($2Al(CH_3)_3 + 3H_2O \rightarrow Al_2O_3 + 6CH_4$) was separated into two half-reactions: (A) $AlOH^* + Al(CH_3)_3 \rightarrow Al\text{-}O\text{-}Al(CH_3)_2^* + CH_4$ and (B) $AlCH_3^* + H_2O \rightarrow AlOH^* + CH_4$, where the asterisks designate the surface species. The trimethylaluminum [$Al(CH_3)_3$] (TMA) and $H_2O$ reactants were employed alternately in an ABAB... binary reaction sequence to deposit the $Al_2O_3$ film. Because each half-reaction is self-limiting, atomic layer controlled $Al_2O_3$ deposition was achieved on the surface of the high aspect ratio pores. To determine the necessary reaction conditions, surface species during each half-reaction were periodically monitored using in situ transmission FTIR spectroscopy. Ex situ gas flux and permporometry measurements were also performed to determine the effect of the binary reaction sequence on the pore diameter. Gas flux measurements for $H_2$ and $N_2$ were consistent with a progressive pore size reduction versus the number of AB reaction cycles. The permporometry measurements showed that the original pore diameter of ∼220 Å was reduced to ∼140 Å after 120 AB reaction cycles.

## Introduction

Reduction and control of pore sizes in membranes are important to achieve gas separations by molecular sieving.[1,2] Chemical vapor deposition techniques are useful for the modification of inorganic membranes. Mesoporous Vycor glass membranes have been modified by the vapor phase decomposition of alkoxysilanes and the $He/O_2$ separation factor increased from 3 to 6.[3,4] This increased separation factor was consistent with a decrease in pore size that changes the mass-transfer mechanism from Knudsen flow to molecular sieving. The pore size in Vycor membranes has also been reduced by the pyrolysis of silicon-containing polymer films.[5,6] A $H_2/SF_6$ separation factor 38 times higher than Knudsen selectivity was reported for the composite membrane. However, reproducibility was a problem because pyrolysis reactions are difficult to control.

The deposition of $ZrO_2$ has also been employed to decrease the pore size in alumina membrane supports.[7] The $ZrO_2$ deposition was achieved using the opposing reactants approach where the two precursors diffuse into the membrane from opposite sides of the porous support.[8] The opposing reactants technique has also been used to deposit silica on Vycor glass membranes. High $H_2/N_2$ selectivities of 250 were acheived with very low permeabilities.[9] Unfortunately, the opposing reactants technique deposits continuously, and deposition is difficult to stop at the optimum pore size.

Temporary carbon barriers have also been used as templates for silica deposition on porous Vycor tubes.[10] The $SiO_2$ deposition was performed by alternating the flow of $SiCl_4$ and $H_2O$ through the tube. Subsequently, the carbon was removed by oxidation, and the resultant porous molecular sieving material displayed $H_2/N_2$ selectivities of 300−8000 at 600 °C. However, the thick top layers of $SiO_2$ on the Vycor tubes imposed a significant resistance to flow that is not suitable for industrial applications.

Dense inorganic membranes have also been prepared by depositing $SiO_2$ on $\gamma$-$Al_2O_3$ supports.[11] Deposition of 1.5−3 $\mu$m of $SiO_2$ using the thermal decomposition of tetraethylorthosilicate (TEOS) yielded $H_2/N_2$ selectivities of 12.6−72 at 600 °C. The deposition of $SiO_2$ using TEOS on $\gamma$-$Al_2O_3$ substrates has also produced thinner separation layers of 0.1−0.05 $\mu$m that achieved $H_2/N_2$ selectivities of over 1000 at 600 °C.[12] Unfortunately, these dense $SiO_2$ membranes are useful only for $H_2$ separation.

Another method that can accomplish these pore size modifications is atomic layer controlled growth using

[⊗] Abstract published in *Advance ACS Abstracts,* February 1, 1997.

(1) Way, J. D.; Roberts, D. L. *Sep. Sci. Technol.* **1992**, *27*, 29.
(2) Hassan, M. H.; Way, J. D.; Thoen, P. M.; Dillon, A. C. *J. Membr.* **1995**, *104*, 27.
(3) Okubo, T.; Inoue, H. *AIChE J.* **1988**, *34*, 1031.
(4) Okubo, T.; Inoue, H. *J. Membr. Sci.* **1989**, *42*, 109.
(5) Li, D.; Hwang, S. T. *J. Membr. Sci.* **1992**, *66*, 119.
(6) Shelekhin, A. B.; Grosgogeat, E. J.; Hwang, S. T. *J. Membr. Sci.* **1992**, *66*, 129.
(7) Lin, Y. S.; Burggraaf, A. J. *AIChE J.* **1992**, *38*, 445.
(8) Tsapatsis, M.; Kim, S.; Nam, S. W.; Gavalas, G. *Ind. Eng. Chem. Res.* **1991**, 2152.
(9) Megiris, C. E.; Glezer, J. H. E. *Ind. Eng. Chem. Res.* **1992**, *31*, 1293.
(10) Jiang, S.; Yan, Y.; Gavalas, G. R. *J. Membr. Sci.* **1995**, *103*, 103.
(11) Wu, J. C. S.; Sabol, H.; Smith, G. W.; Flowers, D. L.; Liu, P. K. T. *J. Membr. Sci.* **1994**, *96*, 275.
(12) Yan, S.; Maeda, H.; Kusakabe, K.; Akiyama, Y. *J. Membr. Sci.* **1995**, *101*, 89.

S0897-4756(96)00377-8 CCC: $14.00 

atomic layer epitaxy (ALE) or atomic layer processing (ALP).[13−15] In the simplest form of atomic layer controlled growth for a two-component film using elemental sources, the adsorption of each element is self-limiting and up to a full monolayer (ML) can be deposited per operational cycle.[13,14] Self-terminating binary reactions have also been used for the controlled deposition of a two component film using molecular precursors.[13−18] An ABAB... reaction sequence was first demonstrated by Suntola and co-workers for the controlled deposition of ZnS films.[16]

When using atomic layer processing, the substrate begins with a reactive functional group on the surface. A precursor containing one of the elements is then introduced and allowed to react with the surface. This reaction adds one layer of the first element and changes the surface functionality. After this reaction occurs, the precursor can no longer react with the surface. Subsequently, the first precursor is pumped away to prevent reactions with the second precursor.

The second precursor is then introduced and can react with the new surface functionality and add the second element of the film. If the precursors are chosen carefully, the surface will have the original functionality prior to the first reaction when this reaction is complete. The second precursor is then pumped away. This sequence can be repeated in an ABAB... sequence to produce any desired film thickness.

The important advantage of ALE/ALP film growth is that the film thickness is dependent not on the kinetics of the reactions but only on the number of reaction cycles. If the half-reactions are allowed to go to completion, variations in the precursor flux to the surface and substrate temperature should not affect the film growth rate. Under ideal circumstances, thin-film growth rates of approximately 1 monolayer/AB reaction cycle should be achieved if the surface functional groups are stable at the reaction temperature.

Many studies have investigated the atomic layer controlled growth of $Al_2O_3$. Most of these investigations have used trimethylaluminum (TMA)[19−26] or trichloroaluminum[27] as the Al source. $H_2O$,[19,20,25,26] $N_2O$,[22] and $H_2O_2$[21,28] have all been used as oxygen sources. Much of this work has concentrated on growing films on flat surfaces for use as high dielectric layers in electronic devices. The deposition of $Al_2O_3$ films to modify filtration membranes is another logical application. Many filtration membranes are made of ceramics and $Al_2O_3$ has very good chemical stability in harsh environments.[29]

The surface chemistry of $Al_2O_3$ film growth has been studied previously on porous alumina membranes using transmission FTIR spectroscopy.[24] In these experiments, the binary reaction $2Al(CH_3)_3 + H_2O \rightarrow Al_2O_3 + 6CH_4$ was separated into two half-reactions:

$$AlOH^* + Al(CH_3)_3 \rightarrow Al{-}O{-}Al(CH_3)_2^* + CH_4 \quad (A)$$

$$AlCH_3^* + H_2O \rightarrow AlOH^* + CH_4 \quad (B)$$

where the asterisks indicate surface species. By monitoring the absorbance of the C−H and O−H stretching vibrations, each reaction was observed to go to completion at 500 K.[24] The measured reaction kinetics were consistent with the reaction mechanisms expressed by the above A and B half-reactions.[24] In addition, the thermal stability studies revealed that the AlOH* and $AlCH_3$* surface coverage decreased approximately linearly versus substrate temperature between 300 and 900 K.

$Al_2O_3$ deposition on Si(100) has also been studied using atomic force microscopy and ellipsometry techniques.[25,26] The atomic force microscopy studies revealed that the above half-reactions produce flat, conformal $Al_2O_3$ thin-film growth.[25,26] Growth rates of ~1.1 Å/AB reaction cycle were also measured with ellipsometry at the optimum reaction temperature of 450 K.[25,26] These ellipsometry studies demonstrated that the growth rates could be correlated with the coverage of reactive functional groups on the surface.

The goal of this paper is to provide a comprehensive study of the modification of $Al_2O_3$ membranes using atomic layer processing techniques. The conformal growth of $Al_2O_3$ films on the internal surfaces of porous membranes should be possible given the previous surface chemistry and growth studies. In situ transmission FTIR spectroscopy was used to monitor the half-reactions on the pore surfaces. Pore size and gas flux were also measured ex situ versus the number of AB reaction cycles. These measurements determined the $Al_2O_3$ deposition rate and demonstrated that the pore size was progressively reduced by $Al_2O_3$ deposition.

## Experimental Section

A new deposition apparatus was used to modify the Anodisc alumina membranes and a complete description of this apparatus will be given elsewhere.[26] In brief, the apparatus consists of a sample load lock chamber, a central deposition chamber, and a high-vacuum surface analysis chamber equipped with a UTI-100C mass spectrometer. These chambers are separated by gate values. A schematic of the central deposition chamber is shown in Figure 1. The arrows in Figure 1 represent the flow of gases through the chamber.

Trimethylaluminum (TMA) is a pyrophoric material and must be handled in an inert atmosphere. The TMA and $H_2O$ liquid reactants were placed in glass coldfingers with Teflon stopcocks. These reactant reservoirs were purified by several

(13) Suntola, T. *Thin Solid Films* **1992**, *216*, 84.
(14) Goodman, C. H. L.; Pessa, M. V. *J. Appl. Phys.* **1986**, *60*, R65.
(15) George, S. M.; Ott, A. W.; Klaus, J. W. *J. Phys. Chem.* **1996**, *100*, 13121.
(16) Pessa, M.; Makela, R.; Suntola, T. *Appl. Phys. Lett.* **1981**, *38*, 131.
(17) Nishizawa, J.; Hitoshi, A.; Kurabayashi, T. *J. Electrochem. Soc.* **1985**, *132*, 1197.
(18) Nishizawa, J.; Kurabayashi, T.; Abe, H. *Surf. Sci.* **1987**, *185*, 249.
(19) Higashi, G. S.; Fleming, C. G. *Appl. Phys. Lett.* **1989**, *55*, 1963.
(20) Soto, C.; Tysoe, W. T. *J. Vac. Sci. Technol. A* **1991**, *9*, 2686.
(21) Fan, J. F.; Sugioka, K.; Toyoda, K. *Jpn. J. Appl. Phys.* **1993**, *30*, L1139.
(22) Kumagai, H.; Toyoda, K.; Matsumoto, M.; Obara, M. *Jpn. J. Appl. Phys.* **1993**, *32*, 6137.
(23) George, S. M.; Sneh, O.; Dillon, A. C.; Wise, M. L.; Ott, A. W.; Okada, L. A.; Way, J. D. *Appl. Surf. Sci.* **1994**, *82/83*, 460.
(24) Dillon, A. C.; Ott, A. W.; Way, J. D.; George, S. M. *Surf. Sci.* **1995**, *322*, 230.
(25) Ott, A. W.; McCarley, K. C.; Klaus, J. W.; Way, J. D.; George, S. M. *Appl. Surf. Sci.* **1996**, *107*, 128.
(26) Ott, A. W.; Klaus, J. W.; Johnson, J. M.; George, S. M. *Thin Solid Films*, in press.
(27) Hiltunen, L.; Kattelus, H.; Leskela, M.; Makela, M.; Niinisto, L.; Nykanen, E.; Soininen, P.; Tiitta, M. *Materials Chem. Phys.* **1991**, *28*, 379.
(28) Kumagai, H.; Matsumoto, M.; Kawamura, Y.; Toyoda, K.; Obara, M. *Jpn. J. Appl. Phys.* **1994**, *33*, 7086.
(29) Bhave, R. R. *Inorganic Membranes-Synthesis, Characterization, and Applications*; Nostrand Reinhold: New York, 1988.

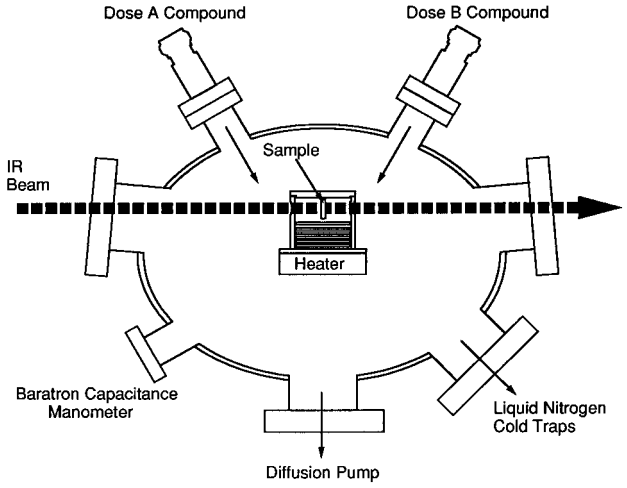


**Figure 1.** Schematic of the central deposition chamber. The arrows represent the direction of gas flow through the chamber.

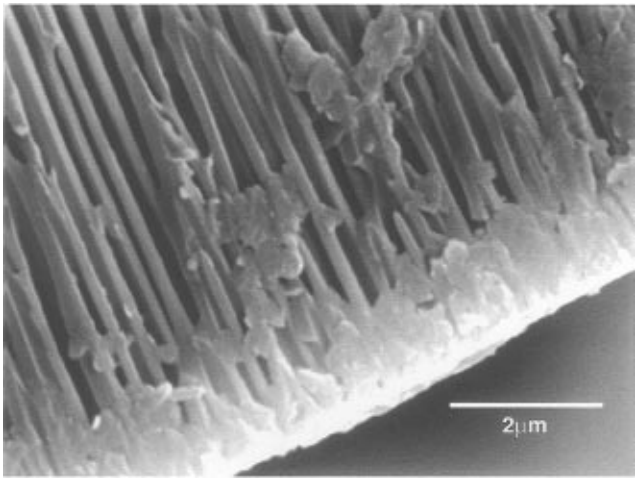


**Figure 2.** Cross-sectional scanning electron micrograph (SEM) of the Anodisc alumina membrane showing the underlying ~2000 Å porous support and the thin ~200 Å porous film on the membrane surface.

freeze−pump−thaw cycles. The reactant gases were introduced into the deposition chamber using two computer controlled valves (Series 9, General Valve).

The central deposition chamber could be pumped with either two liquid $N_2$ traps backed by mechanical pumps or by a 175 L/s diffusion pump equipped with a liquid $N_2$ trap. The two liquid $N_2$ traps were used to pump each precursor separately to avoid mixing and subsequent reaction in the pumps. Transmission FTIR spectroscopy was used to monitor the progress of the reactions on the porous alumina surface.[24] In addition, a small leak from the central deposition chamber to the high-vacuum chamber was used to analyze the gas composition during film growth.

The samples were mounted on a transfer puck (Surface Interface) that could be docked on water-cooled pedestals in either the central deposition chamber or the surface analysis chamber. The docking also connected current and thermocouple feedthroughs that allowed the samples to be heated and temperature-regulated between 300 and 1300 K. A magnetically coupled sample-transfer arm (Surface Interface) moved the puck between the three chambers.

The Anodisc porous alumina filtration membranes were obtained from Whatman Labsales (Hillsboro, OR). These membranes have an asymmetric structure. The majority of the membrane is comprised of ~2000 Å pore diameters with a ~57 $\mu$m thickness. One side of the membrane also contains ~200 Å pore diameters with a ≤2 $\mu$m thickness. A cross-sectional scanning electron microscopy (SEM) picture of the interface between the ~2000 and ~200 Å pores is shown in Figure 2. The alumina membranes were cleaned in a 30% $H_2O_2$ solution at room temperature to remove organic contamination from the surface before insertion in the deposition chamber. A concentrated $HNO_3$ cleaning solution was also utilized and yielded results that were comparable with the 30% $H_2O_2$ cleaning solution.

The alumina membranes were placed in a cassette that was positioned inside an enclosed copper cylinder as described previously.[26] The copper cylinder was then attached to the sample heater on the transfer puck. This copper cylinder with enclosed membranes could be uniformly heated to ~700 K in ~0.5 Torr of any gas. The temperature of the copper cylinder was monitored with a type K thermocouple placed between the cylinder and the transfer puck. Separate experiments showed that the temperature of the membranes in the copper cylinder was identical with the temperature of the copper cylinder. As a final temperature check, the stability of the hydroxyl groups on the membranes in the copper cylinder was in agreement with the previously measured hydroxyl stability on alumina membranes.[24]

In addition to the membranes loaded in the cassette, one alumina membrane was loaded vertically for in situ transmission FTIR studies. The orientation of the IR beam relative to the cassette and vertically mounted sample is shown in Figure 1. The enclosure also was perforated to allow passage of gases. Additional holes provided for the transmission of the infrared beam.

The alumina membranes were heated to 500 K in 10 Torr of $H_2O$ to ensure that all the membranes reached the reaction temperature. The chamber was then pumped to $<1 \times 10^{-5}$ Torr prior to the first TMA exposure. Subsequently, TMA and $H_2O$ were alternately dosed according to the following procedure: Before each dose, the reactant flowed through the chamber until either $H_2O^+$ or $Al(CH_3)_2^+$ was detected on the same scale as $CH_4^+$ by the mass spectrometer using the controlled leak to the analysis chamber. During this period, the inlet valve was left open and the chamber was periodically pumped by the liquid $N_2$ traps. This procedure was necessary to ensure that the reactions with the chamber walls did not consume all the reactants.

Once the reactant flow cycle was completed, the deposition chamber was filled to the reaction pressure of 0.5 Torr and maintained at that pressure for the 1 min reaction time. The reactants were then evacuated using the appropriate liquid $N_2$ trap until the pressure was <10 mTorr. The TMA and $H_2O$ were pumped using two separate pumps to avoid reaction in the pumps. Following this initial pumping, lower pressures of $\sim 3 \times 10^{-5}$ Torr were achieved using the 175 L/s diffusion pump equipped with the liquid $N_2$ trap.

A Nicolet 740 FTIR spectrometer and an MCT-B infrared detector were employed for the in situ vibrational spectroscopic studies.[26] The infrared beam passed through a pair of 0.5 in. thick CsI windows on the central deposition chamber. The CsI windows could be isolated from the chamber using gate valves to prevent species from being deposited inadvertently on the windows. Sensitivity requirements limit transmission FTIR studies to high-surface-area materials. The porous alumina membranes provided a surface area of ~400 $cm^2/cm^2$ that was sufficient for the transmission FTIR studies.[24] All of the spectra presented here were taken with the alumina membranes at 500 K.

For ex situ pore size and gas flux measurements, samples were mounted in a stainless steel, cross-flow membrane holder (Millipore, Medford, MA). The pore size of the alumina membranes was measured before and after the atomic layer controlled deposition using liquid−liquid displacement perm-porometry.[30−32] Briefly, this technique involves saturating the membrane pores with a wetting solvent. The solvent is then

(30) Kim, K. J.; Fane, A. G.; Aim, R. B.; Liu, M. G.; Jonsson, G.; Tessaro, I. C.; Broek, A. P.; Bargeman, D. *J. Membr. Sci.* **1994**, *87*, 35.
(31) Nakao, S. I. *J. Membr. Sci.* **1994**, *96*, 131.
(32) Munari, S.; Bottino, A.; Moretti, P.; Capannelli, G.; Becchi, I. *J. Membr. Sci.* **1989**, *41*, 69.

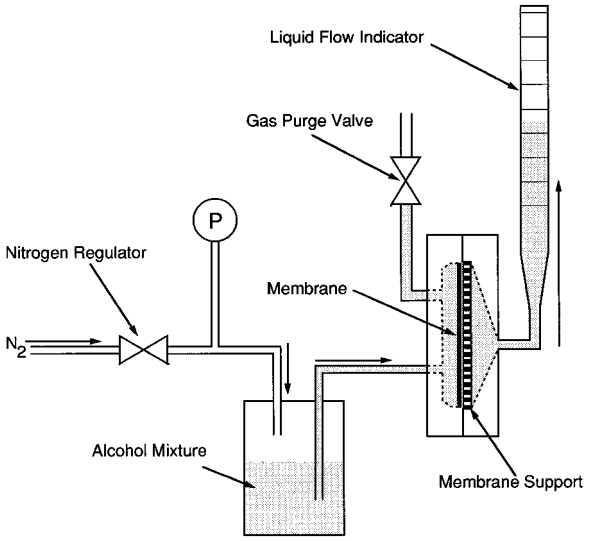


**Figure 3.** Apparatus for the permporometry measurements.

displaced with a second liquid that is immiscible with the wetting solvent. Liquid permeance increases as a function of differential pressure until all of the wetting solvent is displaced from the pores.

Pore diameter, $D_p$, can be obtained using the Cantor equation:[30,32]

$$D_p = 4\sigma/\Delta P$$

where $\sigma$ is the interfacial tension, and $\Delta P$ is equal to the differential pressure required to displace the wetting solvent from the pores of the membrane. This equation assumes that the pore diameter of a capillary is proportional to the curvature of a meniscus formed at the interface of two immiscible liquids. A pore size distribution can be developed by plotting the fractional change of the permeance versus pore diameter. Permeance is defined as flux divided by $\Delta P$ and approaches a maximum when all of the pores are open.[30]

The permporometry apparatus is shown in Figure 3. This apparatus includes a cross-flow cell that allows gases to be purged at the beginning of the experiment. During the permporometry experiment, the membrane is typically saturated with water, then an immiscible alcohol mixture is delivered using a vessel pressurized with nitrogen gas. Solvent flow is measured using a pipette and stop watch. Solvent pressure is measured with an Ashcroft Bourdon gauge.

Certain alcohol−water mixtures are immiscible with water and have very low interfacial tensions in the range $\sigma = 0.35-4.8$ dyn/cm. These low interfacial tensions enable the measurement of pore diameters from the mesopore range ($D_p > 20$ Å) and larger with moderate differential pressures. In these experiments, our immiscible fluid was a mixture of isobutanol, methanol, and water in a 15:7:25 volume ratio with an interfacial tension of $\sigma = 0.35$ dyn/cm.[33]

During permeability measurements, the cross-flow arrangement ensured that the composition of the gas feed to the membranes was constant. Feed and permeate pressures were maintained using back pressure regulators. $H_2$ and $N_2$ gas fluxes were measured at 293 K using bubble flow meters with a pressure differential of 10 psi (520 Torr) across the membrane. The $H_2$ and $N_2$ gases had a purity of 99.999% and were used without further purification.

## Results

The reaction conditions for complete TMA and $H_2O$ half-reactions on the surfaces of ~2000 Å porous Anodisc alumina membranes have been determined previously.[24] The reaction parameters used in this study

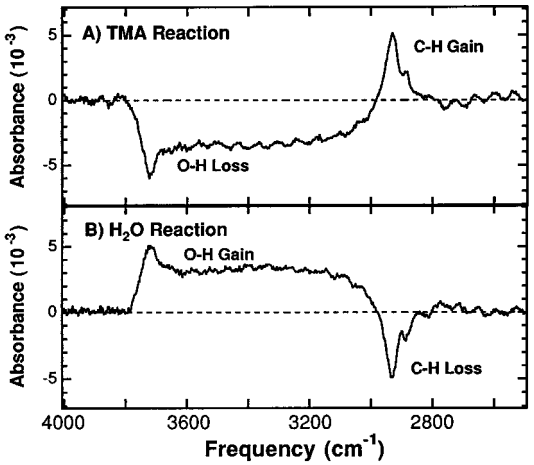


**Figure 4.** (A) FTIR difference spectrum obtained after a saturation TMA exposure at 500 K. This spectrum was referenced to the membrane after the previous $H_2O$ exposure at 500 K. (B) FTIR difference spectrum obtained after a saturation $H_2O$ exposure at 500 K. This spectrum was referenced to the membrane after the previous TMA exposure at 500 K.

were 60 s, 0.5 Torr exposures at 500 K for both TMA and $H_2O$. These AB cycles were performed using the following sequence: flow A/static A (60 s, 0.5 Torr)/evacuate to $<4 \times 10^{-5}$ Torr/flow B/static B (60 s, 0.5 Torr)/evacuate to $<4 \times 10^{-5}$ Torr. The reaction was periodically checked with in situ transmission FTIR spectroscopy to confirm that the $AlCH_3$* coverage remained constant after TMA exposures throughout the experiment. Some of the alumina membranes were removed from the deposition chamber after various numbers of AB cycles.

Figure 4a shows a difference FTIR spectrum after a TMA exposure referenced to the previous $H_2O$ exposure. The negative O−H vibrational stretching feature (3800−2600 $cm^{-1}$) indicates that hydroxyl groups on the surface after a $H_2O$ exposure are removed by the subsequent TMA exposure. Concurrently, the number of methyl groups on the surface increases from zero to a saturation value during the TMA exposure and the C−H vibrational stretching feature (2940−2840 $cm^{-1}$) appears as a positive feature. This reaction will not occur on the *as-received* Anodisc alumina membranes without the $H_2O_2$ cleaning procedure. Increasing the exposure time has no affect on the spectra and indicates that the reaction has reached saturation. When the spectrum is referenced to the CsI windows, a positive hydroxyl feature is observed after multiple AB reaction cycles. This cumulative hydroxyl feature will be discussed in more detail below.

A difference FTIR spectrum after an $H_2O$ exposure referenced to the previous TMA exposure is displayed in Figure 4b. This figure shows the inverse of Figure 4a. In this case, methyl groups are removed by the $H_2O$ exposure and the C−H vibrational stretching region has a negative absorbance. The O−H vibrational stretching region also shows a positive absorbance because of the increased number of hydroxyl groups on the surface. Increasing the exposure time results in no spectral change and reveals that the reaction has reached saturation. After each $H_2O$ exposure, no methyl feature is observed when the spectra is referenced to the CsI windows. This behavior indicates that the reaction has

(33) Capannelli, G.; Vigo, F.; Munari, S. *J. Membr. Sci.* **1983**, *15*, 289.

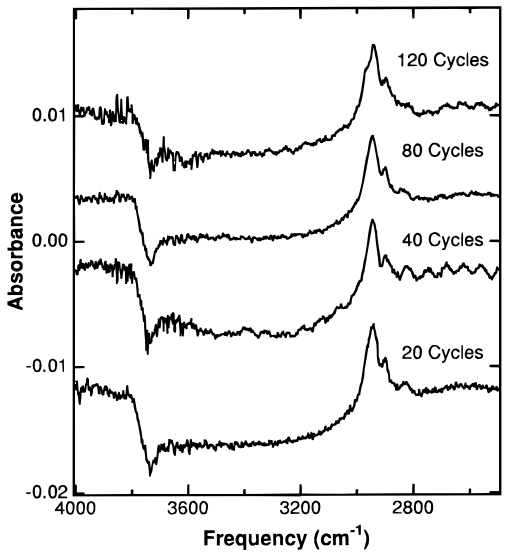


**Figure 5.** FTIR difference spectra recorded after saturation TMA exposures at 20, 40, 80, and 120 AB cycles. Each spectrum is referenced to the membrane after the previous $H_2O$ exposure.

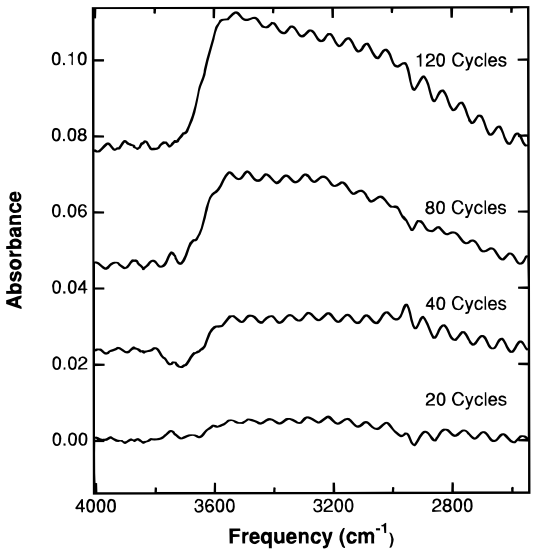


**Figure 6.** FTIR spectra after saturation $H_2O$ exposures at 20, 40, 80, and 120 AB cycles. Each spectrum is referenced to the membrane after the initial $H_2O$ exposure at 500 K.

gone to completion, and there is no cumulative methyl feature.

As the pore size is reduced, the conductance of the membrane is lower, and longer exposures may be required for the reactions to reach completion. To determine if the reaction continues to saturate as a function of AB reaction cycles, the cycles were periodically stopped and IR spectra were taken after both the $H_2O$ and TMA exposures. Figure 5 shows difference spectra after TMA exposures referenced to the previous $H_2O$ exposure after 20, 40, 80, and 120 AB cycles. In each case, the spectra appear similar to Figure 4a. In addition, the integrated absorbance from the C−H stretching vibration after the TMA exposure does not change with either number of AB cycles or increasing TMA exposure time.

Figure 6 shows the FTIR spectra after $H_2O$ exposures referenced to the initial alumina membrane after 20, 40, 80, and 120 AB reaction cycles. A progressive

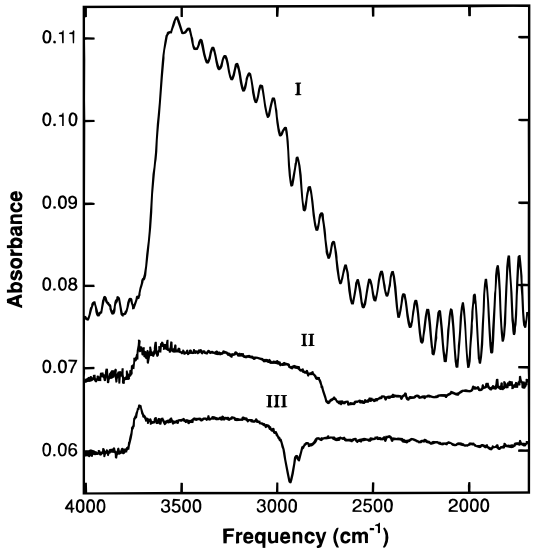


**Figure 7.** (I) FTIR spectrum obtained after a saturation $H_2O$ exposure at 120 AB cycles referenced to the membrane after the initial $H_2O$ exposure at 500 K. (II) FTIR difference spectrum recorded after a saturation $H_2O$ exposure referenced to the membrane after the previous saturation $D_2O$ exposure. (III) FTIR spectrum obtained after a saturation $H_2O$ exposure referenced to the membrane after the previous saturation TMA exposure.

increase in the absorbance by the AlO−H stretching vibrations is observed as a function of AB reaction cycles. This increase indicates a growth of hydroxyl groups in or on the deposited $Al_2O_3$ film. To determine whether these new hydroxyl groups were on the surface or incorporated in the bulk $Al_2O_3$ film, isotope-exchange experiments were performed with $D_2O$.

The FTIR spectrum I in Figure 7 displays the hydroxyl feature after 120 AB cycles referenced to the original alumina membrane. This spectrum represents the total number of hydroxyls incorporated in or on the deposited $Al_2O_3$ film. In addition, difference spectra taken after $H_2O$ exposures are shown in FTIR spectra II and III. These spectra are referenced to the spectra of alumina membranes after previous saturation $D_2O$ and TMA exposures. The FTIR spectrum II displays the number of AlOH groups that can be produced by isotopic exchange of AlOD groups. The FTIR spectrum III reveals the number of AlOH groups that can be produced by $H_2O$ reaction with $AlCH_3$ groups.

The AlO−H vibrational stretching features in spectra II and III are similar. These features represent only surface species that can be produced by isotopic exchange or the TMA reaction. These spectra are much smaller in total absorbance than the AlO−H stretching features in FTIR spectrum I. This comparison argues that the cumulative AlO−H vibrational stretching spectrum I represents primarily AlOH species in the bulk of the $Al_2O_3$ film.

The pore diameter was measured for each of the alumina membranes using liquid−liquid displacement permporometry. Figure 8 shows the pore-size distribution of the alumina membrane after 0, 40, 76, and 116 AB cycles. These pore-size distributions were measured for two separate deposition experiments and were consistent for the first and second batch of samples. For the second experiment, Figure 8 shows that the initial pore diameter was ∼223 Å with an upper limit for the half-height width of ±7 Å. After 116 AB reaction cycles,

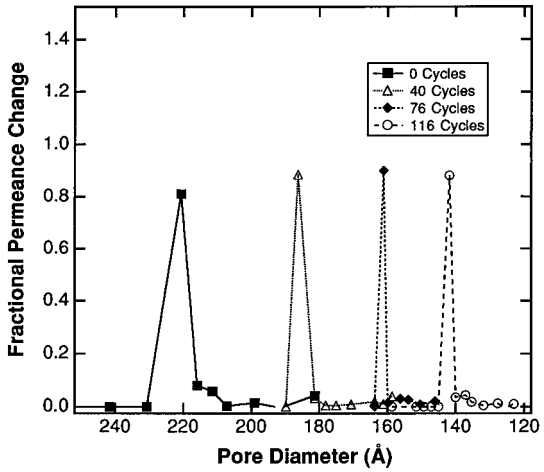


**Figure 8.** Fractional change in the permeance versus pore diameter after 0, 40, 76, and 116 AB cycles as measured by permporometry.

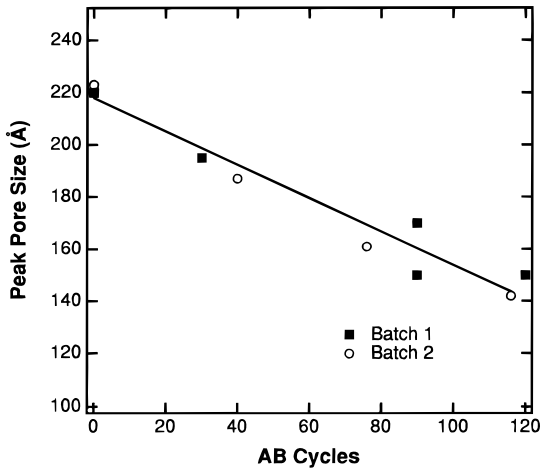


**Figure 9.** Peak pore diameter versus number of AB cycles measured using liquid−liquid displacement permporometry.

the pore diameter was ~142 Å with an upper limit for the half-height width of ±3 Å. The measured distribution of pore diameters is currently only as narrow as the spacing between the data points. Figure 8 shows that the distribution does not broaden versus AB reaction cycles.

A plot of the peak pore diameter versus number of AB cycles is displayed in Figure 9. The pore diameter decreases nearly linearly with the number of AB reaction cycles. Linear regression of the data from both experiments indicates that the pore diameter is reduced at a rate of 0.73 Å/cycle. This pore diameter reduction is consistent with a $Al_2O_3$ growth rate on the surface of the pores of 0.37 Å/cycle.

Figure 10 shows a decrease in the $N_2$ permeance versus the number of AB cycles. The $H_2$ and $N_2$ gas fluxes through each membrane were measured at a feed pressure of 1140 Torr. A differential pressure of 520 Torr existed between the feed and permeate. The permeance values were not equivalent for the first and second experiments. Samples from the first experiment exhibited higher fluxes than samples from the second experiment. These differences are attributed to variations in membrane thickness and porosity from different production batches of the Anodisc membranes. However, the decrease in permeance versus number of AB cycles was reproducible. The $H_2/N_2$ gas permeability

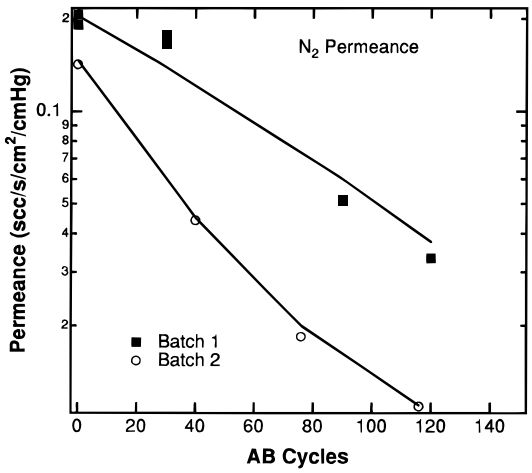


**Figure 10.** $N_2$ gas permeance through the alumina membranes versus number of AB cycles measured at a differential pressure of 520 Torr.

ratio, i.e., the $H_2/N_2$ separation factor, also remained nearly constant at 3.1 ± 0.2 for all of the modified membranes.

There may be significant adsorption of airborne organics that results in pore blockage within the modified membranes. Though this fouling is not fully understood, a substantial decrease in permeability was observed for the modified membranes versus time. This decrease persisted even after repeated cleaning in nitric acid and/or boiling $H_2O_2$. However, there was no large scale contamination on the membranes observed by scanning electron microscopy. To avoid the possible adsorption of organics, the porosimetry and permeability tests for samples from the second experiment were performed within a few days after deposition and removal from the vacuum chamber. These tests resulted in much less scatter in the data.

## Discussion

Previous thin-film growth studies on single-crystal Si(100) have demonstrated that conformal deposition of $Al_2O_3$ can be achieved using binary reaction sequence chemistry.[25,26] Deposition on the high aspect ratio porous alumina membranes provides a more severe test for this atomic layer controlled growth technique. In the asymmetric alumina membrane, the aspect ratios are ≤100:1 in the ~200 Å pores with a length of ≤2 $\mu$m and ~285:1 in the ~2000 Å pores with a length of ~57 $\mu$m. The small pores will also have an extremely low conductance that will necessitate long reactant exposures for the reaction to reach completion.

Self-limiting chemistry provides for conformal and atomic layer controlled deposition in the high aspect ratio pores of the alumina membrane. The surface reactions will first occur at the opening of the pore. After the surface area close to the opening of the pore has been passivated, the precursors are able to travel deeper into the pore. As a result, the reaction will progress down the pore walls until the reaction goes to completion over the entire surface area.

Figure 4 shows that the A and B reactions are occurring on the alumina membrane surface. These results are consistent with previous FTIR studies that demonstrated that both half-reactions go to completion at 500 K.[24] In the previous study, the membranes were cleaned with a 1000 K anneal and then rehydroxylated.

This process removed all the hydroxyl groups, including the inaccessible AlOH groups. The rehydroxylation then only replaced the surface hydroxyl groups. This preparation procedure was unacceptable for this study because the annealed membranes became brittle and very difficult to handle.

To avoid the 1000 K anneal, the membranes in this study were cleaned in a 30% peroxide solution to remove organic contamination from the surface. The membranes were unreactive without this cleaning procedure. With this cleaning method, the hydroxyl groups on the surface became reactive, but the buried hydroxyl groups were not removed from the film. These inaccessible AlOH groups were not reactive, but their presence complicated the interpretation of the FTIR spectra.

Figure 6 shows that the number of hydroxyl groups in the membrane is also constantly increasing as a function of AB reaction cycles. This behavior is attributed to AlOH groups accumulating in the $Al_2O_3$ film. Isotopic substitution and reaction experiments were performed to distinguish surface AlOH species and AlOH species in the $Al_2O_3$ film. Hydroxyl groups on the surface can be replaced with AlOD or $AlOAl(CH_3)_2$ species through proton exchange or reaction with TMA, respectively:

$$AlOH^* + D_2O \rightarrow AlOD^* + HDO$$

$$AlOH^* + Al(CH_3)_3 \rightarrow Al{-}O{-}Al(CH_3)_2^* + CH_4$$

The surface can then be rehydroxylated by reaction with $H_2O$.

Inaccessible hydroxyl groups will not be reactive with either $D_2O$ or TMA. Spectrum II in Figure 7 shows that ~15% of the accumulated AlOH* groups after 120 AB cycles could be isotope-exchanged with $D_2O$ and then rehydroxylated. Likewise, spectrum III reveals that ~15% of the accumulated AlOH* species could also be reacted with TMA and then rehydroxylated. This behavior indicates that ~85% of the accumulated AlOH* groups that build up after 120 AB reaction cycles are buried in the $Al_2O_3$ film.

The growth rate on the surface of the alumina pores is 0.37 Å/AB reaction cycle. In comparison, the measured growth rate on single-crystal Si(100) at 500 K was 1.0 Å per AB cycle.[26] The different growth rates may reflect the differences between the starting surfaces. The initial surface on Si(100) is a hydroxylated $SiO_2$ film produced by exposing a hydrogen-terminated Si(100) surface to an $H_2O$ plasma at room temperature.[26] The initial surface in the porous alumina membrane is a hydroxylated amorphous $Al_2O_3$ surface. These different initial surfaces may evolve different growing $Al_2O_3$ surfaces.

The slower growth rates in the ~200 Å pores may also reveal different reaction kinetics and reaction mechanisms in the confined structure of the smaller pores. The ~200 Å pores have a smaller radius of curvature than the ~2000 Å pores. This smaller radius of curvature may position neighboring hydroxyl groups closer together and possibly reduce their thermal stability. The thermal stability of hydroxyl groups measured on the ~2000 Å pores was previously utilized to explain the temperature-dependent $Al_2O_3$ growth rates on the Si(100) substrate.[26] A reduction in hydroxyl stability on the smaller pores would also be expected to lead to slower $Al_2O_3$ growth rates.

Figure 5 shows that the TMA reaction remains nearly constant from 20 to 120 AB reaction cycles. This reaction continues to reach completion after the same TMA exposure and is not affected by the pore size reduction from ~220 to ~120 Å. This behavior is attributed to the geometry of the asymmetric alumina membrane. The membrane is composed of a 57 $\mu$m thick support with ~2000 Å pores and a $\leq 2$ $\mu$m thick layer with ~200 Å pores. As a result, most of the surface area in the alumina membrane is in the 57 $\mu$m thick support, and the transmitted infrared beam will be most sensitive to this surface area. Because the pore size of the support is estimated to be reduced from ~2000 to ~1900 Å, the total surface area of the membrane is reduced by only ~10%. The conductance of gases in these ~1900−2000 Å pores also does not change significantly. Consequently, the FTIR study of the TMA reaction may not be extremely sensitive to the pore reduction from ~220 to ~120 Å.

Although the A and B half-reactions saturate according to the FTIR measurements, these spectra are dominated by the surface area of the ~2000 Å pores. The saturation behavior for the ~200 Å porous region of the asymmetric membrane may be different. Consequently, there is a chance that the surface reactions in the ~200 Å pores are not reaching completion. This possibility may also explain the lower growth rate of 0.37 Å/AB reaction cycle.

The reduction in pore diameter and decrease in gas permeance versus number of AB reaction cycles shown in Figures 9 and 10 indicate that the binary reaction sequence chemistry is progresively depositing $Al_2O_3$ in the alumina pores. In addition, Figure 8 reveals that the pore reduction occurs without an increase in pore size distribution. This behavior illustrates that highly controlled and conformal deposition can be achieved in pores with high aspect ratios using binary reaction sequence chemistry. The high aspect ratio of the pores limits the gas conductance into the pores. This low conductance only increases the required exposure time that is required for the surface reactions to reach completion.

The $H_2/N_2$ separation factor of $3.2 \pm 0.2$ is somewhat lower than the ideal separation factor of 3.74 that would be expected for molecular flow of pure gases through the membranes. The ideal separation factor, due to Knudsen diffusion or molecular flow, reflects the ratio of the mean molecular velocities, $\nu_{H_2}/\nu_{N_2}$, and is proportional to $(M_{N_2}/M_{H_2})^{1/2}$. The ideal separation factor will not be observed until the Knudsen number is >100.[34] The Knudsen number is the ratio of the mean free path of the gas to the pore diameter. Given a mean free path of ~100 Å at 293 K and 1140 Torr and an initial pore diameter of 220 Å, the initial Knudsen number is ~0.5. Therefore, the observed separation factor is attributed to mixed molecular and viscous flow through the ≤220 Å pores in the alumina membranes. Similar behavior has been observed previously for mixed molecular and viscous flow through the pores of ceramic membranes.[29]

(34) Barrer, R. M. *Zeolites and Clay Materials as Sorbents of Molecular Sieves*; Academic Press: London, England, 1978.

## Conclusions

Sequential surface chemical reactions were used to obtain controlled and conformal $Al_2O_3$ deposition on porous alumina substrates. In this approach, the binary reaction $2Al(CH_3)_3 + 3H_2O \rightarrow Al_2O_3 + 6CH_4$ was separated into two half-reactions:

$$AlOH^* + Al(CH_3)_3 \rightarrow Al{-}O{-}Al(CH_3)_2^* + CH_4 \quad (A)$$

$$AlCH_3^* + H_2O \rightarrow AlOH^* + CH_4 \quad (B)$$

where the asterisks identify the surface species. Transmission FTIR spectroscopy was used to monitor the reactions. Both reactions were observed to reach completion versus reactant exposure time, but hydroxyl groups were progressively incorporated into the deposited $Al_2O_3$ film.

Liquid−liquid permporometry experiments showed that the pores of an Anodisc alumina membrane can be progressively reduced from ∼220 to ∼140 Å after 120 AB reaction cycles. This pore reduction is consistent with an $Al_2O_3$ growth rate of 0.37 Å/AB cycle on the surface of the pores. This growth rate is less than the observed growth rate of 1.0 Å/AB cycle on Si(100) at 500 K. This lower growth rate in the porous alumina membrane may be attributed to conductance limitations or reduced hydroxyl stability in the smaller pores.

Gas flux measurements were consistent with a decreasing permeance as a function of AB reaction cycles. The separation factor for $H_2/N_2$ of $3.2 \pm 0.2$ was explained by a combination of mixed molecular and viscous flow through the pores of the alumina membrane. These experiments indicate that the binary reaction sequence chemistry for $Al_2O_3$ deposition can be employed to grow films with atomic layer control on extremely high aspect ratio structures.

**Acknowledgment.** This work was supported by the Office of Naval Research under Contract N00014-92-J-1353 and exploratory research grants from Chevron Research and Engineering Company to S.M.G. and J.D.W. J.D.W. and K.C.M. are also supported by the Department of Energy Office of Basic Energy Sciences, Department of Chemical Sciences under Grant DE-FG03-93ER14363.

CM960377X